Available online at www.sciencedirect.com
SCIENCE DIRECT
Pattern Recognition 39 (2006) 1401 – 1414
PATTERN RECOGNITION
THE JOURNAL OF THE PATTERN RECOGNITION SOCIETY
www.elsevier.com/locate/patcog

Integration of fuzzy spatial relations in deformable models— Application to brain MRI segmentation

Olivier Colliot*, Oscar Camara, Isabelle Bloch

École Nationale Supérieure des Télécommunications, Département TSI, CNRS UMR 5141 LTCI, 46, rue Barrault, 75634 Paris Cedex 13, France

Received 1 July 2005; received in revised form 18 October 2005; accepted 20 February 2006

Abstract

This paper presents a general framework to integrate a new type of constraints, based on spatial relations, in deformable models. In the proposed approach, spatial relations are represented as fuzzy subsets of the image space and incorporated in the deformable model as a new external force. Three methods to construct an external force from a fuzzy set representing a spatial relation are introduced and discussed. This framework is then used to segment brain subcortical structures in magnetic resonance images (MRI). A training step is proposed to estimate the main parameters defining the relations. The results demonstrate that the introduction of spatial relations in a deformable model can substantially improve the segmentation of structures with low contrast and ill-defined boundaries.

Keywords: Spatial relations; Deformable models; Fuzzy sets; MRI; Subcortical structures

1. Introduction

Spatial relations constitute the basic elements contained in linguistic descriptions of spatial configurations and describe the organization of the different objects in an image. These relations are usually classified into different types including topological, distance and directional relations [1]. Their importance has been highlighted in many domains related to computer science and engineering, such as artificial intelligence [1], computational linguistics [2], geographic information systems [3] or autonomous robotics [4].

In image analysis and pattern recognition, these relations provide structural knowledge by opposition to image features such as gray level or texture. Their ability to describe scenes [5,6] makes them potentially useful for a wide range of imaging applications including aerial imaging [5,7], face recognition [8] and medical imaging. Moreover, being close in essence to the natural language description, they can be easily understood and manipulated by a non-technical user who will then be able to interact more efficiently with image analysis procedures.

The analysis of brain magnetic resonance images (MRI) is a typical example of imaging application in which spatial relations can be useful. Indeed, the human brain is a structured scene and spatial relations are ubiquitous in natural language descriptions found in neuroanatomy textbooks [9]. Furthermore, relations between brain structures are more stable among individual subjects and less dependent on the acquisition parameters than the characteristics of the structures themselves. They can thus be a source a robustness for automated procedures.

Fuzzy sets constitute an appealing framework to represent spatial relations. Indeed, since they correspond to linguistic propositions, spatial relations are often intrinsically imprecise and fuzzy sets allow modeling this imprecision. The satisfaction of a given relation will then be defined as a matter of degree rather than in an "all-or-nothing" manner. Moreover, fuzzy sets provide a common framework to represent different types of individual spatial relations. In particular, the relations can be easily combined using fuzzy fusion operators. The fuzzy set framework has been used to represent different types of spatial relations including

* Corresponding author. Tel.: +33 1 45 81 80 91; fax: +33 1 45 81 37 94.
E-mail addresses: Olivier.Colliot@enst.fr (O. Colliot), o.camara-rey@ucl.ac.uk (O. Camara), Isabelle.Bloch@enst.fr (I. Bloch).

0031-3203/$30.00
doi:10.1016/j.patcog.2006.02.022

adjacencies [10], distances [11], directions [12], symmetries [13] and complex relationships such as "between" [14].

Spatial relations have been used in a relatively small number of pattern recognition applications. Keller and Wang [5] used spatial relations to automatically generate linguistic descriptions of images. Le Ber and Mangelinck [7] used topological relations to analyze satellite images. A handwritten recognition system based on directional relations has been proposed by Wang et al. [15]. Géraud et al. [16–18] have proposed to use fuzzy spatial relations for brain structure recognition on MRI. These relations were subsequently used for the same application in [19] in which they were combined to a possibilistic clustering method using a fusion framework. In all these applications, spatial relations were used for high-level tasks (i.e. recognition) and not directly integrated in the segmentation itself which was based only on image characteristics. However, spatial relations could be of great help to find the contours of poorly contrasted objects, with ill-defined boundaries or sharing similar intensities with their neighbors.

Several segmentation approaches implicitly integrate the spatial relationships between the objects of a scene. Atlas-based methods, e.g. [20,21], compute a nonlinear transformation between the target image and a labeled template. In such a way, the relations between the objects in the template are implicitly modeled. Point distribution models, which are used in active shape models [22], can infer not only the shape of individual objects but also the relations between them from a training set of instances. However, in these approaches, the spatial relations are defined implicitly in either the template or the training set and are not specified individually. We propose a different approach which aims at integrating explicitly individual spatial relations in the segmentation process. This should allow to model more directly expert knowledge expressed as linguistic descriptions and to explicitly choose the constraints which will be included in the segmentation, for example keeping only the relations which are anatomically meaningful.

Deformable models [23] refer to a large class of computer vision methods and have proved to be a successful segmentation technique [24] for a wide range of applications. Moreover, they constitute an appropriate framework for merging heterogeneous information such as image features and spatial relations. However, the accuracy of the segmentation results can be deteriorated when strong edges are lacking in the image. In those cases, the deformable model may leak through the boundaries of the objects. Spatial relations could help overcoming this difficulty by providing additional information about the spatial extension of the objects.

In this paper, we thus propose a methodology to introduce prior constraints based on fuzzy spatial relations in a deformable model. Spatial relations are represented as fuzzy subsets of the image space and are integrated in the deformable model as a new external force. The proposed framework is then used to segment brain subcortical structures in MRI. Our experiments show that adding spatial relations to a deformable model can prevent it from being attracted by contours of irrelevant objects and from progressing beyond the limits of structures with weak boundaries.

This paper is organized as follows. In Section 2, we briefly review the underlying principles of deformable models and present computational representations of spatial relations. Section 3 is devoted to the combination of spatial relations and deformable models. In Section 4, the proposed framework is applied to the segmentation of brain subcortical structures in MRI.

2. Background

2.1. Deformable models

Deformable models [23], also called active contours or snakes, are curves or surfaces evolving within an image from a starting point to a final state that should correspond to the target object (i.e. the object we want to segment). Two types of information drive the evolution: a data term that attracts the model towards the edges of the image and a regularization term that forces the model to stay smooth and regular. The evolution of a deformable model can be written as the minimization of the following energy [23]:

$$E(\mathbf{X}) = E_{int}(\mathbf{X}) + E_{ext}(\mathbf{X}), \tag{1}$$

where $\mathbf{X}$ is the deformable contour (or surface in 3D), E_{int} is the internal energy that specifies the regularity of the contour and E_{ext} is the external energy that drives the contour towards image edges. The external energy is computed by integrating on the contour a potential P that should be minimum on image edges: $E_{ext}(\mathbf{X}) = \int_{[0,1]} P(\mathbf{X})\, \mathrm{d}s$. In the original formulation [23], the potential P is derived from the image gradient.

The evolution can also be described by the following dynamic force equation [24]:

$$\gamma \frac{\partial \mathbf{X}}{\partial t} = \mathbf{F}_{int}(\mathbf{X}) + \mathbf{F}_{ext}(\mathbf{X}), \tag{2}$$

where $\mathbf{F}_{int}$ is the internal force and $\mathbf{F}_{ext}$ the external force. This expression is linked to the energetic formulation by $\mathbf{F}_{ext}(\mathbf{X}) = -\nabla P(\mathbf{X})$. However, this equation is more general since it allows using external forces that do not derive from an energy potential.

A considerable amount of research has been carried out on deformable models. Different external forces have been proposed to provide more robustness and a broader attraction range than the image gradient, e.g. [25,26]. Region-based forces have been designed and applied to the segmentation of textured images [27]. Furthermore, several authors have introduced prior shape constraints in deformable models, e.g. [22,28,29]. More details are beyond the scope of this paper and can be found in Refs. [24,29].

On the contrary, to our knowledge, fuzzy spatial relations have never been introduced in this context. Xu et al. [30] used

a force computed from fuzzy sets in a deformable model. However, these fuzzy sets were derived from image features and not from structural knowledge. They represented a degree of membership to gray-level classes (of gray and white matter in a cortex reconstruction application) obtained with a fuzzy classification. Pitiot et al. [31] introduced a deformable model driven by expert knowledge. They presented a general evolution framework which allows including heterogeneous information composed of shape, texture and distance constraints. In particular, they proposed to compute a force from distance relations. Nevertheless, they did not consider other types of spatial relations such as directions. On the contrary, our aim is to take advantage of the common framework provided by fuzzy sets to propose a force construction method that can be used for different types of spatial relations.

2.2. Spatial relations

2.2.1. Representation approaches

We consider spatial relations that define the position of a *target* object with respect to a *reference* object. To illustrate our purpose, let us provide some examples of spatial relations between brain structures:

- *direction*: the left (respectively, right) thalamus is *on the left* (resp. right) of the third ventricle and *below* the lateral ventricle;
- *distance*: the caudate nucleus is *near* the lateralventricle.

In these two examples, the caudate nucleus and the thalamus are target objects and their position is defined with respect to the ventricles, which are chosen as reference objects. For example, to segment the thalamus, our aim will be to constrain the deformable model to satisfy the spatial relations *on the left* of the third ventricle and *below* the lateral ventricle.

In order to integrate spatial relations in deformable models, it is first necessary to provide a computational representation of the relations. Approaches for representing spatial relations can be divided into qualitative and quantitative methods. The first ones often rely on formal logic [1,32,33] and do not seem appropriate for an integration in a numerical setting such as deformable models. On the contrary, quantitative methods provide a numerical evaluation of the relations. An additional distinction can be made between quantitative methods: a first type of approach evaluates spatial relations between two given objects; a second type defines the satisfaction of a relation, with respect to a given reference object, at each point of the space. The first one has been applied to a large number of relations, including fuzzy adjacencies [10], distances [11], symmetries between fuzzy objects [13] and the representation of directional relative position based on the histograms of angles [34] or forces [35]. Nevertheless, this type of approach is not suitable to our problem since our aim is to make the deformable model evolve towards the points where the relation is fulfilled. It is thus necessary to compute the degree of satisfaction of the relation at each point of the space.

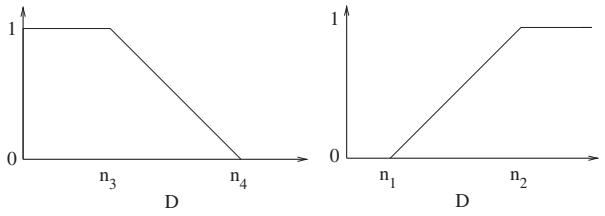

Fig. 1. Fuzzy intervals on the set of distances corresponding to relations "near" and "far from".

We make use of the second type of approach in which spatial relationships are represented as fuzzy subsets of the image space (2D or 3D). In the present work, directional and distance relations are considered. However, the framework is general and other types of relations could be integrated, the only restriction being that they must be modeled as spatial fuzzy sets.

2.2.2. Distances

For distance relations such as "near", "at a distance approximately equal to", "far from", we define a fuzzy interval f of trapezoidal shape on the set of distances $\mathbb{R}^+$ [36] (Fig. 1). The kernel of f is defined as $[n_2, n_3]$ and its support as $[n_1, n_4]$, where $0 \leqslant n_1 \leqslant n_2 \leqslant n_3 \leqslant n_4$. For the relation "near" one has $n_1 = n_2 = 0$, and n_3 and n_4 are defined according to prior knowledge on the largest distance from a point in the target object to a point in the reference object. Similarly, for the relation "far from", n_1 and n_2 are defined according to the smallest distance. To obtain a fuzzy subset of the image space, f is combined with a distance map d_A to the reference object A:

$$\mu_d(P) = f(d_A(P)), \tag{3}$$

where P is a point of the space. Fig. 2(a) presents an example of a fuzzy set corresponding to a distance relation.

2.2.3. Directions

Directional relations are represented using the fuzzy landscape approach [12]. Let $\mathbf{u}$ be a unit vector corresponding to the direction under consideration, let P be a point of the space, Q a point of the reference object A and $\beta(P, Q)$ the angle between vectors $\mathbf{QP}$ and $\mathbf{u}$ computed in $[0, \pi]$. We then define, for every point P:

$$\beta_{min}(P) = \min_{Q \in A} \beta(P, Q). \tag{4}$$

The fuzzy subset of the image space representing the relation is

$$\mu_\alpha(P) = g(\beta_{min}(P)), \tag{5}$$

where g is a decreasing function from $[0, \pi]$ to $[0, 1]$. A common choice for g is $g(\theta) = \max[0, 1 - (2/\pi)\theta]$. More generally, one can choose a trapezoidal interval, like in the

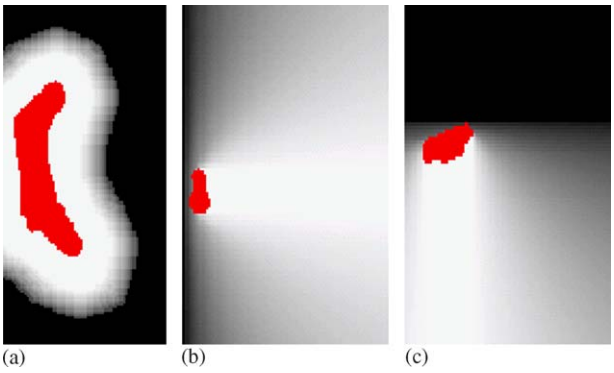

Fig. 2. Fuzzy sets representing distance and directional relations. (a) Distance: "near the lateral ventricle". The reference object is superimposed on the fuzzy set. The values of the fuzzy set decrease when going away from the reference object. (b) Direction: "on the left of the third ventricle". Values of the fuzzy set decrease when going away from the direction under consideration. (c) Direction: "below the lateral ventricle". In all the figures, we represent spatial fuzzy sets with the convention: "bright areas correspond to high values".

case of distances, or a trigonometric function. In Section 4.3, a learning procedure is proposed to estimate the parameters defining functions f and g. Examples of fuzzy sets representing directions are shown in Figs. 2(b) and (c).

3. Integration framework

3.1. Overview

Our purpose is to introduce spatial relations in the evolution scheme of a deformable model. We choose the dynamic force formulation of the evolution (Eq. (2)) because it is more flexible in the choice of the external term. We propose to represent a spatial relation as a new force that will constrain the deformable model to fulfill the relation. The external force $\mathbf{F}_{ext}$ in Eq. (2) is replaced with a force describing both edge information and structural constraints:

$$\mathbf{F}_{ext} = \lambda \mathbf{F}_C + \nu \mathbf{F}_R, \tag{6}$$

where $\mathbf{F}_C$ is a classical data term that will drive the model towards the edges, $\mathbf{F}_R$ is a force associated to spatial relations and λ and ν are weighting coefficients.

Since a spatial relation is represented by a fuzzy subset of the image space, we will propose a method to construct the force $\mathbf{F}_R$ from a fuzzy set. When several relations are involved in the description of the target object, they are combined using fusion operations between fuzzy sets [37]. The combination of several relations will thus be represented by a single force, corresponding to the fuzzy set obtained by the fusion. In the following, we will use t-norms for conjunctive fusion and t-conorms for disjunctive combination [38]. The choice of a particular t-norm or t-conorm depends on the degree of severity or indulgence that is required for the fusion. We use the t-norm "minimum" and "product" which correspond to indulgent conjunctions. Fig. 3(a) shows an example of conjunction using a t-norm of the fuzzy sets presented in Figs. 2(b) and (c).

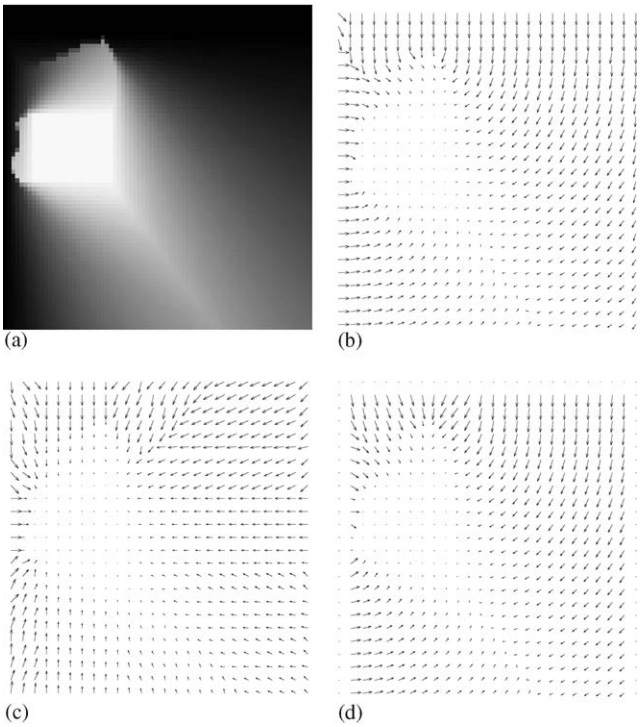

Fig. 3. Computation of a force from a fuzzy set corresponding to spatial relations. (a) The fuzzy set representing the conjunction of spatial relations "on the left of the third ventricle and below the lateral ventricle". The fuzzy set corresponds to the fusion of the sets presented in Figs. 2(b, c), using the t-norm "product". (b) Force $\mathbf{F}_R^1$ using the fuzzy set as an energy potential. (c) Force $\mathbf{F}_R^2$ using a distance potential force. (d) Force $\mathbf{F}_R^3$ using a gradient diffusion technique. The three forces are directed towards the points of the space where the relation is fulfilled. To enhance visualization, forces are displayed with a $\frac{1}{3}$ under-sampling.

3.2. Construction of the force $\mathbf{F}_R$

3.2.1. Required properties

Let R be a fuzzy set representing a spatial relation (or a combination of relations) and μ_R its membership function. The force $\mathbf{F}_R$ should drive the deformable model towards regions where the relation is fulfilled and thus be directed towards high values of μ_R. When the relation is completely satisfied, the model should be driven by edge information only, i.e. $\mathbf{F}_R$ should be zero in the kernel of R. The less the relation is satisfied, the higher the modulus of the force should be, thus we impose it to be proportional to $(1-\mu_R)$. Finally, the computation time for the force should be reasonable. In the following, we propose three different construction methods for $\mathbf{F}_R$ that fulfill these properties.

3.2.2. Using the fuzzy set as a potential

A first idea could be to derive an energy potential directly from the fuzzy set, e.g. $P_R = 1 - \mu_R$, leading to a potential

force $\mathbf{F}_R = -\nabla P_R$. However, such a force would obviously have zero values outside the support of R, which is highly undesirable as the relation is completely unsatisfied in this region. This can be solved by adding to the potential the distance from the support, then defining:

$$P_R^1(P) = 1 - \mu_R(P) + d_{supp(R)}(P), \tag{7}$$

where $d_{supp(R)}$ is the distance from the support of R. With the following normalization, the force is proportional to $(1-\mu_R)$, as required in the properties:

$$\mathbf{F}_R^1(P) = -(1-\mu_R(P))\frac{\nabla P_R^1(P)}{\|\nabla P_R^1(P)\|}. \tag{8}$$

An example of external force computed using this approach is shown in Fig. 3(b).

3.2.3. Using a distance potential force

Distance potential forces [25], defining a potential as a function of a distance map to a binary edge detector, provide a broad attraction range, which is of interest in our case since $\mathbf{F}_R$ should be non-zero everywhere outside the kernel of R. Nevertheless, since we want to replace the edge map with the fuzzy set, we need to use a fuzzy distance instead of a classical one. For instance, good properties would be obtained with the fuzzy morphological distance [11]:

$$d_v = 1 - D_v(\mu_R), \tag{9}$$

where v is a structuring element with radial symmetry: $v(x,y,z) = 1 - \sqrt{x^2+y^2+z^2}/k$ and k is the size of this element.

A potential would then be defined as

$$P_R(P) = g(d_v(P)), \tag{10}$$

where g is a non-decreasing function, e.g. $g(x) = -1/x$.

However, the morphological distance is computationally expensive. For 3D applications, we recommend to replace it with a classical distance such as the distance to the kernel of R:

$$P_R^2(P) = g(d_{Ker(R)}(P)), \tag{11}$$

where $d_{Ker(R)}(P)$ is a distance map to the kernel of R. The corresponding force, denoted by $\mathbf{F}_R^2$, is computed using the same formula as in Eq. (8). Fig. 3(c) presents a force constructed using this equation.

3.2.4. Using a gradient diffusion technique

Using a gradient vector diffusion technique also allows having a wide attraction range. The gradient vector flow (GVF), introduced by Xu et al. [26], computes a smooth vector field while being close to the original gradient in the regions where it has high values. Here, we replace the edge map with our fuzzy set μ_R in the GVF formulation. The GVF is the vector field v that corresponds to the steady-state of the following equation:

$$\begin{cases} \dfrac{\partial v}{\partial t} = c\nabla^2 v - \|\nabla\mu_R\|^2(v - \nabla\mu_R), \\ v(P,0) = \nabla\mu_R(P). \end{cases} \tag{12}$$

The first equation is a combination of a diffusion term that will produce a smooth vector field and a data term that forces v to stay close to $\nabla\mu_R$. The parameter c defines the trade-off between the two terms. In regions where $\|\nabla\mu_R\|$ is low, the diffusion term will prevail. In particular, inside the kernel and outside the support of R, only diffusion will occur, giving a non-zero force. However, as we want the force to be zero in the kernel, we will use the following normalization:

$$\mathbf{F}_R^3 = (1-\mu_R)\frac{\mathbf{u}}{\|\mathbf{u}\|}, \tag{13}$$

where $\mathbf{u}$ is the GVF. An example of this force is shown in Fig. 3(d).

3.3. Example

In order to illustrate the role of spatial relations in a deformable model, Fig. 4 presents a basic example on a synthetic 2D image representing a portion of the brain (extracted from the BrainWeb database[1]). The goal is to segment the caudate nucleus. The evolution is governed by a regularization term (the one proposed by Kass et al. [23]), a data term and a spatial relation force. The data term is a GVF [26] computed on an edge map and drives the model towards the contours of the image (Fig. 4(b)). The spatial relation force constrains the result to be "to the right of the ventricle" (Fig. 4(c)). Here we present the force $\mathbf{F}_R^3$ but the same segmentation results were obtained with the other methods. These two forces are combined using Eq. (6) (Fig. 4(d)). When only data and regularization terms are considered (Fig. 4(e)), the model is attracted by the first strong edges that it encounters. On the contrary, when the spatial relation term is added (Fig. 4(f)), the deformable contour avoids objects that do not fulfill the relation and converges towards the target one. This example illustrates that spatial relations can prevent deformable models to be attracted by the contours of irrelevant objects and allow initializing them far from the target structures.

3.4. Discussion

The three proposed forces fulfill the required properties but they are not equivalent.

First, $\mathbf{F}_R^1$ and $\mathbf{F}_R^3$ are directed towards increasing values of μ_R because they are computed using the gradient of the fuzzy set. In the particular case of a fuzzy set with local maxima outside its kernel, they point towards these maxima.

[1] http://www.bic.mni.mcgill.ca/brainweb/

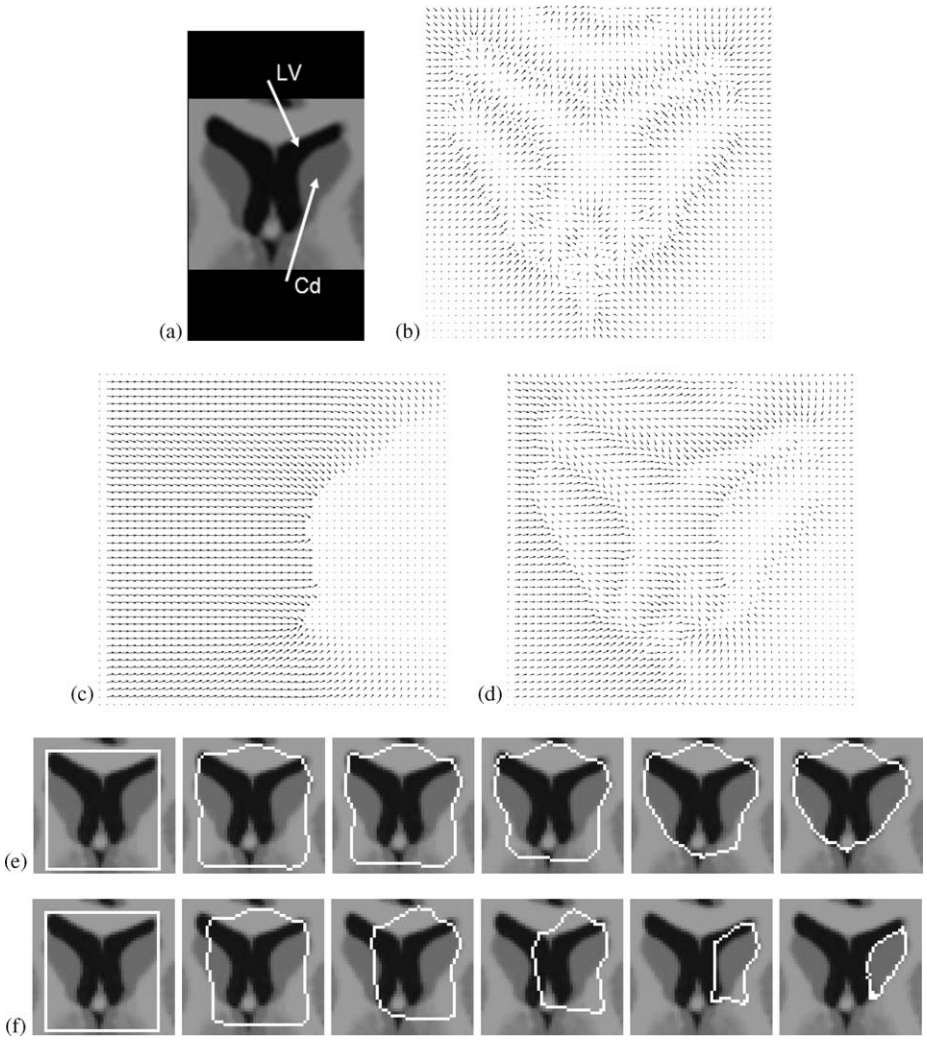

Fig. 4. Basic example of deformable model driven by spatial relations. (a) The image is a portion of a simulated brain MRI and shows the lateral ventricles (LV) and the caudate nuclei (Cd). The target object is the right caudate nucleus. (b) Data term that drives the deformable model towards the edges of the image (a gradient vector flow). (c) Force $\mathbf{F}_R^3$ representing the spatial relation "to the right of the ventricle (in black on the image)". (d) Combination of the two previous forces using Eq. (6). (e) Evolution: using only the data term and starting from the white rectangle on the left image, the deformable model is attracted by the first strong edges that it encounters. (f) Using the combination of both the data term and the spatial relation, it is able to converge towards the caudate nucleus.

On the contrary, $\mathbf{F}_R^2$ is always directed towards the kernel of R. These differences can be appreciated in Fig. 3. Moreover, whereas $\mathbf{F}_R^1$ and $\mathbf{F}_R^2$ are computed directly from the fuzzy set or from its kernel, $\mathbf{F}_R^3$ introduces an additional regularization. Finally, the computational cost of $\mathbf{F}_R^1$ and $\mathbf{F}_R^2$ is very low (5 s for a $128 \times 128 \times 124$ image on a PC Pentium III 1 GHz). The computation time is higher for $\mathbf{F}_R^3$ (3 min), while staying reasonable, this being the price for regularization.

The choice of one of these three forces will depend on the application at hand. If the fuzzy set has local maxima and if one wants the deformable model to be attracted by these maxima, $\mathbf{F}_R^1$ or $\mathbf{F}_R^3$ should be used. On the contrary, if these local maxima are thought to represent unreliable information and the target object should be found inside the kernel of μ_R, it is preferable to use $\mathbf{F}_R^2$. Finally, if such maxima are not present, the three forces should lead to similar results. Moreover, if the computational speed is a crucial requirement of the application, $\mathbf{F}_R^1$ or $\mathbf{F}_R^2$ will be preferred. On the contrary, if one wants to obtain a smoother force, to correct possible imperfections of μ_R, $\mathbf{F}_R^3$ can be used.

An additional comment concerns the combination scheme proposed in Eq. (6). It is also possible to use the fuzzy set as a weighting function for the data term, thus not taking the latter into account where the relation is completely unfulfilled:

$$\mathbf{F}_{ext} = \lambda \mu_R \mathbf{F}_C + v\mathbf{F}_R. \tag{14}$$

It should be noted that all these results are also valid with a crisp set instead of a fuzzy one. In that case, forces $\mathbf{F}_R^1$ and $\mathbf{F}_R^2$ are equal since their support is identical to their kernel.

The proposed framework is valid in two or three dimensions. Moreover, it does not depend on the choice of the

internal force, of the data term or of the geometry of the deformable surface. In the next section, we choose a discrete representation based on simplex meshes [39] and a data term built using the GVF [26].

4. Application to the segmentation of brain structures in MRI

We applied the proposed framework to the segmentation of brain subcortical structures in T1-weighted MRI. The method is sequential: each structure is segmented separately relying on the spatial relations with respect to previously obtained structures. The core of our method is composed of a 3D deformable model, constrained by spatial relations between brain structures as proposed in the previous section.

We segmented the caudate nuclei, the thalami, the lateral ventricles and the third ventricle. Since they are well-contrasted and easier to segment, the ventricles are extracted first and are used as reference objects for segmenting the caudate and the thalamus. The principle of the method is general and can be applied to other structures.

4.1. 3D deformable model

To implement the deformable surface in three dimensions, we choose a discrete representation based on simplex meshes which allows a fast convergence of the model and a simple discretization of the internal force. Simplex meshes, introduced by Delingette [39], are topologically dual to triangulations and have a constant vertex connectivity.

4.1.1. Evolution

The evolution of the deformable surface $\mathbf{S}$ is driven by the following equation:

$$\gamma \frac{\partial \mathbf{S}}{\partial t} = \mathbf{F}_{int}(\mathbf{S}) + \mathbf{F}_{ext}(\mathbf{S}). \tag{15}$$

$\mathbf{F}_{int}$ is the internal force controlling the regularity of the surface:

$$\mathbf{F}_{int} = \alpha \nabla^2 \mathbf{S} - \beta \nabla^2 (\nabla^2 \mathbf{S}), \tag{16}$$

where α and β, respectively, control the surface tension (prevent it from stretching) and rigidity (prevent it from bending) and ∇^2 is the Laplacian operator. It is then discretized on the simplex mesh using the finite difference method [40].

$\mathbf{F}_{ext}$ is the external force and represents the combination of a data term and a force corresponding to a spatial relation, as proposed in Section 3:

$$\mathbf{F}_{ext} = \lambda \mathbf{F}_C + \nu \mathbf{F}_R. \tag{17}$$

$\mathbf{F}_R$ is a force associated to spatial relations. In the following experiments, this force has been computed using the first method $\mathbf{F}_R^1$. However, similar results would be obtained with the two other approaches since the fuzzy sets that we consider do not possess local maxima outside their kernel. The spatial relations that define the force F_R correspond to anatomical descriptions of the gray nuclei, defined in collaboration with a neuroanatomist [41]:

- *caudate nucleus*: near and to the left (or right) of the lateral ventricle;
- *thalamus*: to the left (or right) of the third ventricle and below the lateral ventricle.

The data term $\mathbf{F}_C$ is a GVF [26], computed from an edge map, which produces a broad attraction range and allows progressing into boundary concavities. In the next section, we propose an original method to compute an edge map for the gray nuclei.

4.1.2. Edge map computation

Two main difficulties appear when detecting the edges of the gray nuclei in MRI: the noise and the lack of contrast of the gray/white interface. Linear spatial filtering which is usually associated to Canny–Deriche edge detectors [42] is inadequate in this case as it would mix contours of thin elongated objects such as the caudate nucleus. Anisotropic diffusion [43] is an efficient way to remove noise in homogeneous regions while preserving and even enhancing edges. However, due to the poorly defined borders of the gray nuclei, this edge enhancement is insufficient.

We propose to enhance edges by computing the gradient on a probability map indicating for each voxel its membership to a given structure. This probability is computed as

$$P(x) = p(I(x)), \tag{18}$$

where I is our image. Its gradient is related to the gradient of I by

$$\nabla P(x) = p'(I(x)) \nabla I(x), \tag{19}$$

where p' is the first-order derivative of p. This means that edge enhancement will occur in the neighborhood of the extrema of p'. If we choose p to be a Gaussian function $G_{m,\sigma}$ of mean m and standard-deviation σ, edges will be enhanced in the neighborhood of $m \pm \sigma$. The mean intensity m_N and the standard deviation σ_N corresponding to a given nucleus N are computed using a modeling of the radiometric characteristics of the gray nuclei as a function of the intensities of gray and white matter [44]. We then empirically choose to enhance the transition between the gray nuclei and the ventricles at $m_N - 2\sigma_N$ and the transition with the white matter at $m_N + \sigma_N$.

To reduce the noise, we finally apply an anisotropic diffusion on the probability map. Applying it on the map rather than on the original image has the additional advantage to normalize the image, allowing choosing the same diffusion parameter for all images. Fig. 5 presents an edge map computed for the caudate nucleus and the corresponding GVF,

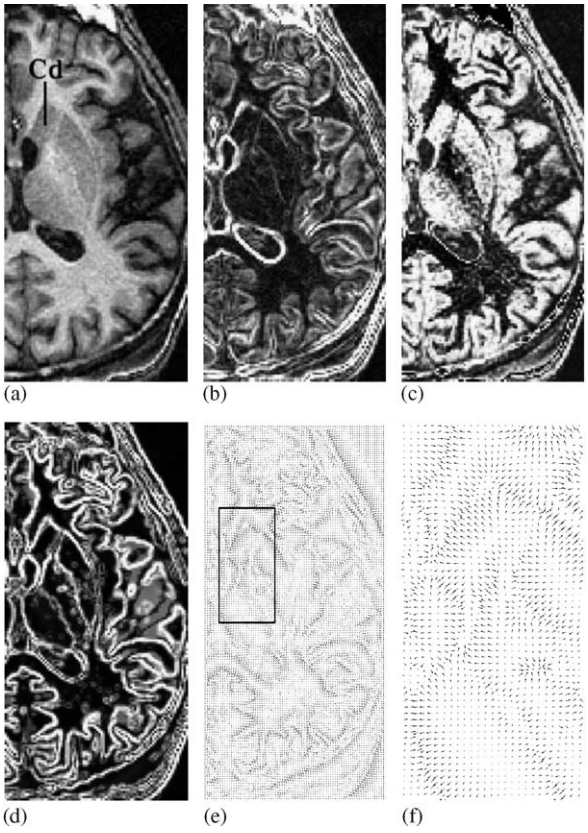

Fig. 5. Edge map for the caudate nucleus (axial slices): (a) original image (the caudate nucleus is indicated by the label "Cd"), (b) gradient computed on the original image, (c) probability map, (d) edge map: gradient computed on the probability map after anisotropic diffusion, (e) gradient vector flow (GVF) computed on the previous edge map, (f) zoom on a portion of the GVF.

which is used as the data term $\mathbf{F}_C$ in the deformable model evolution.

4.1.3. Initialization

In order to obtain a faster and more accurate convergence of the deformable model, we construct an initial segmentation that is used as a starting point for the evolution. This step is composed of simple thresholding and morphological operations and also makes use of spatial relations describing the target object. This initial segmentation is illustrated in the case of the caudate nucleus in Fig. 6.

First, a region of interest (ROI) is constructed to restrict the search of the target structure (Fig. 6(a)). This ROI is defined by the fuzzy set corresponding to the relations that should be satisfied by the target object. If a single relation is involved in the description of the structure, the ROI is defined by the fuzzy set corresponding to this relation. When several spatial relations are involved, the ROI corresponds to the fusion of the fuzzy sets representing these relations (see Section 3.1 for the description of fusion operations). As for the ventricles, the ROI is the region "far from the brain surface". For the right (resp. left) caudate nucleus, the ROI corresponds to the region "near and on the right (resp. left) of the lateral ventricle". For the right (resp. left) thalamus, it is defined as "below the lateral ventricle and to the right (resp. left) of the third ventricle" (this corresponds to the descriptions given in Section 4.1.1).

An automatic thresholding is then performed in the ROI (Fig. 6(b)). For the ventricles, the threshold range is $[0, m_{GM} - 2\sigma_{GM}]$, where m_{GM} and σ_{GM} are the mean and standard deviation of the gray matter. For the caudate and the thalamus, the threshold values are $m_N - \sigma_N$ and $m_N + \sigma_N$, where m_N and σ_N are the radiometric characteristics of the considered gray nucleus, estimated as for the edge map (Section 4.1.2). These values were chosen empirically on the available acquisition sequences. They should not be critical as the segmentation will be refined with the deformable model.

We then need to separate the different objects extracted by the thresholding and to select the one we want to segment (Fig. 6(c)). To this purpose, we use a morphological opening, whose optimal size is found iteratively. Openings of increasing size are computed successively until a connected component matching the characteristics of the object is found. At each step, an opening of a given size is performed and the connected components are extracted. If one of the components matches the characteristics of the target object, this component is chosen. If none of the components verify this condition, the process is iterated with a larger opening. The sizes of the openings are successively: 6-, 18-, 26-connectivity, 2 mm, ... The characteristics which are used to select the components are composed of the spatial relations associated to the target object as well as its size and/or position. Specifically, for the ventricles, we used the size and position. For the caudate and the thalamus, we used the size and the spatial relations. Threshold values for these characteristics were roughly tuned manually. They do not seem sensitive since we used the same values for all images. Moreover, for the size and the position, we chose the thresholds in a very tolerant manner to account for their variability.

Finally, possible holes in the previous results are filled with a morphological closing and we obtain the initial segmentation (Fig. 6(d)). The iterative procedure together with the post-processing proved to be robust and adapted to all our test images.

This segmentation is then transformed into a triangulation using an isosurface algorithm based on tetrahedra [45]. It is decimated and converted to a simplex mesh by the dual operation. Finally, its topological quality is optimized to make faces regular. This simplex mesh is used as the starting point of the deformable model (Fig. 6(e)).

It should be noted that for the ventricles, we do not make use of the deformable model evolution. Indeed these structures are well-contrasted and the initial segmentation proved sufficient for our purpose which is to provide a reference for the processing of the gray nuclei.

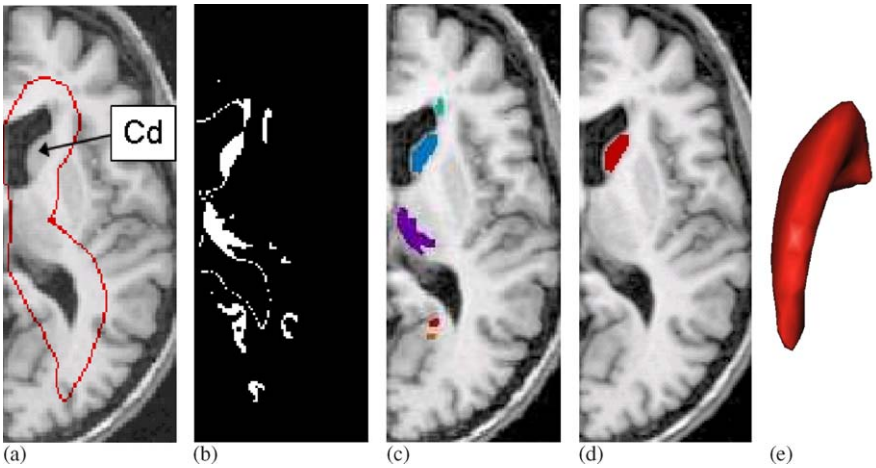

Fig. 6. Initialization for the caudate nucleus (axial slices): (a) contour of the kernel of the region of interest superimposed on the MRI (the caudate is indicated by the arrow); (b) automatic thresholding in the region of interest; (c) separation of objects using a morphological opening of optimal size and selection of the target object; (d) initial segmentation; (e) simplex mesh corresponding to this initial segmentation.

4.2. Pre-processing

The following pre-processing steps are applied prior to the segmentation of brain structures. Images are first linearly registered into a common stereotaxic space [46], which allows roughly normalizing the position and size of structures that are used to construct the initialization. MR images are then corrected for intensity non-uniformity [47], which produces consistent intensities for the different tissues throughout the volume. Finally, the brain is extracted using a robust method based on morphological operations [48]. This eliminates radiometric classes that are of no interest to our application (scalp, air, skull…). Nevertheless, whereas we systematically use the non-uniformity correction before extracting the brain, we suggest not to use it for the gray nuclei because their contrast is altered by this correction.

4.3. Parameter learning

Parameter tuning is an important step in segmentation procedures. Even though we had obtained good results with only a rough manual tuning [41], more robustness can be obtained using a learning of the parameters on a training set of manually segmented structures. In particular, we propose to estimate the parameters involved in the construction of the fuzzy sets corresponding to distances and directions. As we will see from the experiments (Section 4.4), the others parameters of the method are not critical and thus do not need a training.

For a given spatial relation, the parameters should be set so that the corresponding fuzzy set enclose the target object. The parameters involved in the computation of distances and directions are the ones that define the functions f and g in Eqs. (3) and (5). These functions are fuzzy intervals of trapezoidal shape. Their kernel and their support are defined based on the maximum (or minimum) distance or angle.

For the distance relation "near", the training consists in the computation of the maximum distance from a point P of the target object B to the reference object A:

$$d_{max} = \max_{P \in B}(d_A(P)). \tag{20}$$

Similarly, for the relation "far from", the minimum distance d_{min} is computed.

For directions, we calculate the maximum value of $\beta_{min}(P)$ (as defined by Eq. (4)) for points P in the target object B:

$$\beta_{max} = \max_{P \in B}(\beta_{min}(P)). \tag{21}$$

For the training set, the mean m and standard deviation σ of d_{max}, d_{min} or β_{max} (depending on the type of spatial relation) are computed. Using these values, fuzzy intervals f and g are chosen with kernel $[0, m]$ and support $[0, m + 2\sigma]$ to take into account the possible variability of the parameters in the training set.

4.4. Results and discussion

4.4.1. Parameter learning

The training was performed for the caudate nucleus which was manually segmented in 10 MRI. Spatial relations describing the caudate are as follows: it should be "near" and "on the left (resp. right)" of the ventricle. Therefore, for each of them, we calculated the maximum distance d_{max} and angle β_{max}. The mean m and standard deviation σ of d_{max} and β_{max} were then computed. Results are presented in Table 1.

The spatial relations defining the thalamus are the directions "to the left (resp. right) of the third ventricle" and "below the lateral ventricle". No training was performed for this structure and we obtained satisfactory results by using

Table 1
Results of the training of the parameters involved in the definition of spatial relations for the caudate nucleus

	Left hemisphere	Right hemisphere
d_{max} (in mm)	13.8 ± 1.5	13.4 ± 1.3
β_{max} (in radians)	1.1 ± 0.1	1.03 ± 0.1

Values are shown as $m \pm \sigma$, where m is the mean and σ the standard-deviation.

$g(\theta) = \max[0, 1 - (2/\pi)\theta]$ which is a common choice for directional relations (see Section 2.2.3).

4.4.2. Segmentation results

We segmented the lateral ventricles, the third ventricle, the caudate nuclei and the thalami in 10 T1-weighted MRI. Results were visually inspected and were found to satisfactorily delineate the structures (an example is shown in Fig. 7). The ventricles are not very difficult to segment as they possess a high contrast with surrounding structures. The caudate nucleus and the thalamus are much more challenging since their boundaries are often weak and ill-defined. Most parts of the caudate were accurately delineated. In particular, it was successfully separated from neighboring structures such as the putamen and the nucleus accumbens, thanks to the spatial relations. The only exception concerned the posterior part of the body and the tail which are very thin structures, usually not processed in automated methods [21,28] (the tail was also excluded from the manual segmentations as done in [31]). As for the thalamus, the edge map we proposed in Section 4.1.2 proved to be very useful, providing a much stronger gradient than if it would have been computed from the original image. Moreover, its lower limit is uneasy to find and the relation with respect to the third ventricle has helped to provide an adequate initialization to the deformable model. Finally, the deformable model corrected the irregularities of the initial result.

In the case of the caudate nucleus, we performed a quantitative validation by comparing automated and manual segmentations on the 10 images of the training set. Parameters were estimated using a "leave-one-out" approach: for the processing of a given image, the training was done only on the 9 others. This strategy allows using the training set as a test group without introducing any bias in the result.

Results were quantitatively assessed using the following measures. We made use of the similarity index [49,21], which is a special case of kappa statistic:

$$S = \frac{2|M \cap A|}{|M| + |A|}, \tag{22}$$

where M is the manual label, A is the automatic one and $|.|$ is the cardinal. This measure is sensitive to variations in shape, size and position. We also computed error measures derived from the partial Hausdorff distance and the mean absolute distance between automatic and manual contours, as proposed in [31]. Given the previous manual and automatic labels, denoted as M and A, respectively, the asymmetric Hausdorff distance between the corresponding manual and automatic contours M_c and A_c is defined as

$$H_{asym}(M_c, A_c) = \max_{x \in M_c} \left(\min_{y \in A_c} d_E(x, y) \right), \tag{23}$$

where $d_E(x, y)$ is the Euclidean distance between points x and y. The symmetric Hausdorff distance is then defined as the maximum of $H_{asym}(M_c, A_c)$ and $H_{asym}(A_c, M_c)$. However, as pointed out in [31], this measure is highly sensitive to outliers and we thus considered the 95th percentile of the symmetric Hausdorff distance.[2] Similarly, we also computed a symmetric mean absolute distance by taking the average of the mean absolute distances from M_c to A_c and from A_c to M_c.

Table 2 presents the results of the evaluation. The mean similarity was 0.87 which corresponds to a strong agreement between manual and automated segmentations. The 95th percentile of the symmetric Hausdorff distance and the mean absolute distance were 2.2 and 1 mm, respectively, which indicates that, for the vast majority of points, the contours of the automated segmentations closely follow those of the manual labels.

The similarity index obtained with our method in the case of the caudate nucleus is close to those reported in Refs. [21] (0.86) and [50] (0.91). The 95th percentile of the symmetric Hausdorff distance and the mean absolute distance are similar to those obtained by Pitiot et al. [31], when including all constraints—distance, shape and texture—in their system (distance values of 2.0 and 1.6 mm, respectively). However, comparisons between different segmentation approaches must be done cautiously since their evaluations rely on different datasets and possibly different acquisition protocols.

Table 2 also presents the results obtained with the initial segmentation. As expected, it can be seen that the deformable model provides a much better result than the initialization, the 95th percentile decreasing from 5.1 to 2.2 mm and the similarity index increasing from 0.79 to 0.87. The initial segmentation, which also makes use of spatial relations to define a ROI, provides a reasonable first approximation of the caudate nucleus. In a few cases, we assessed the influence of the initialization on the final result by dilating or eroding the initial segmentation. We found that the final result is not very sensitive to initial overestimations (i.e. when the initialization is dilated), because the spatial relation force pulls back the deformable model. On the contrary, it may be more sensitive to underestimations (i.e. erosions), because narrow parts of the caudate nucleus cannot be recovered by the deformable model, this being mainly due to the internal force. The aim of the initial segmentation is precisely to address this issue by providing a starting point that allows converging into these narrow regions.

[2] It should be noted that this 95th percentile no longer satisfies the definition of a distance.

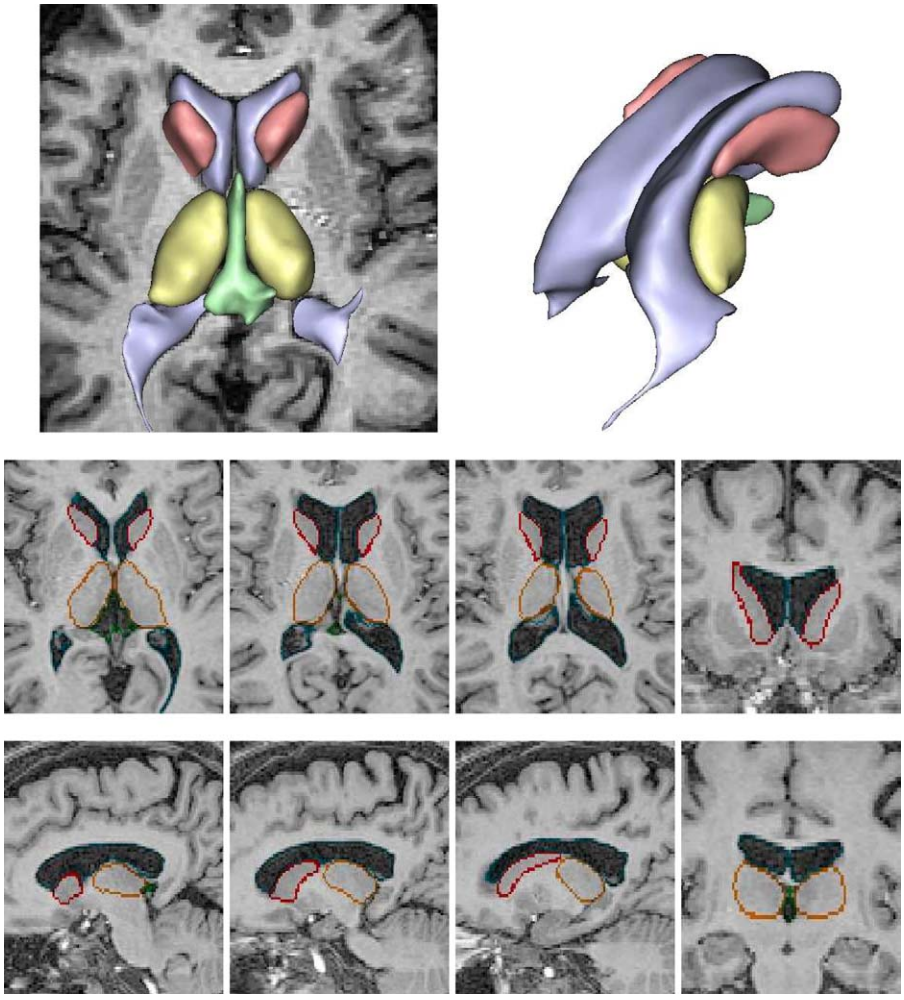

Fig. 7. Results obtained for the lateral ventricles, the third ventricle, the caudate nuclei and the thalami. Top: 3D rendering superimposed on an axial slice. Bottom: structure contours superimposed on axial, sagittal and coronal slices. 3D images have been visualized using the Anatomist software (www.anatomist.info), developed at SHFJ, Orsay, France.

Table 2
Evaluation of the segmentation of the caudate nucleus

	95th percent. (in mm)	Mean dist. (in mm)	Similarity index
Final result	2.2 ± 0.9 (1.4–4.4)	1.0 ± 0.3 (0.7–1.5)	0.87±0.02 (0.81–0.90)
Initialization	5.1 ± 2.0 (2.0–8.9)	1.5 ± 0.5 (0.8–2.7)	0.79±0.03 (0.72–0.84)
Without F_R	6.1 ± 4.6 (1.4–13.9)	1.8 ± 1.1 (0.7–3.7)	0.80±0.08 (0.66–0.89)

The table reports the values of the 95th percentile of the symmetrized Hausdorff distance, the mean absolute distance and the similarity index S. In each cell, the results obtained on the 20 caudate nuclei (10 images and 2 hemispheres) are reported as mean±standard-deviation with the range in parentheses. The upper row indicates the result obtained with our method. The middle one indicates the results obtained with the initial segmentation. The lower row indicates the results that would be obtained without the force F_R corresponding to the spatial relations.

Since it is difficult and tedious to obtain manual annotations of the images, the quantitative evaluation was performed only for the caudate nucleus. However, a simple visual examination of the segmentation of the thalamus confirms, in a qualitative way, the good results obtained with the proposed method.

4.4.3. Contribution of spatial relations

To assess the contribution of the integration of spatial relations in the deformable model, we compared our results to those that would be obtained without the force F_R corresponding to the spatial relations. As shown in Fig. 8, without the spatial relations, the deformable model may converge beyond the limit of the caudate, into neighboring structures such as the putamen and the nucleus accumbens. Table 2 presents the results that would be obtained without the force F_R. The 95th percentile of the symmetrized Hausdorff distance is much higher, with a mean of 6.1 mm and a maximum of 13.9 mm, indicating that the deformable model

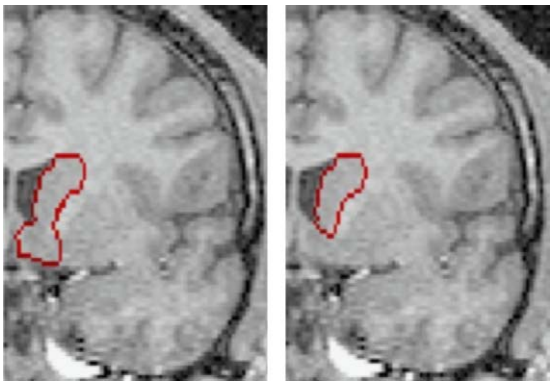

Fig. 8. Influence of spatial relations on the evolution of the deformable model. The force corresponding to spatial relations prevents the model from converging beyond the limit of the structure. Left: result obtained without the spatial relations. Right: result obtained with the spatial relations.

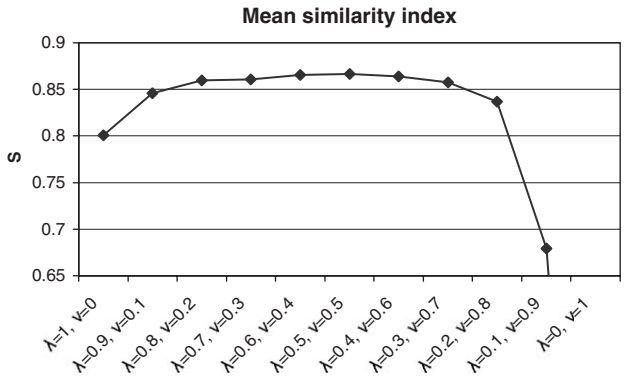

Fig. 9. Mean similarity indices obtained for different values of the parameters λ and ν attached to the trade-off between the data term F_C and the spatial relations force F_R in Eq. (17). With $\lambda + \nu = 1$, λ and ν vary between 0 and 1. The similarity is very stable for $\lambda \in [0.3; 0.8]$ (and thus $\nu \in [0.2; 0.7]$), the difference being smaller than 0.01. Outside this interval, the similarity is strongly decreased (the value corresponding to $\lambda = 0$ is $S = 0$ but is not shown to facilitate visualization).

has progressed beyond the boundary of the structure. The similarity index can also be severely decreased, going as low as 0.66. The spatial relations are thus a key element of the robustness of the method.

4.4.4. *Influence of parameters*

To conclude this section, let us comment on the tuning of the parameters. For the initial segmentation, the size of the morphological opening was iteratively estimated. The characteristics of the extracted objects were automatically checked to match those of the target structure thus ensuring that the object has been disconnected from its neighbors.

For the deformable model, regularization parameters are not sensitive since we used the same parameters for all images. It is also the case of the ones involved in the definition of the data term. The spatial relation parameters have been estimated in a training phase and they are highly stable (Section 4.3).

Finally, we evaluated the influence of the parameters that are specific to the integration of spatial relations in the deformable model. These are the parameters λ and ν attached to the trade-off between the data term F_C and the spatial relations force F_R in Eq. (17). For this evaluation, we computed the similarity that is obtained for the caudate nucleus with values of λ and ν between 0 and 1 (Fig. 9). The results were very stable for values $\lambda \in [0.3; 0.8]$ (and thus $\nu \in [0.2; 0.7]$). The wide range of acceptable values for these parameters show that they are not sensitive. This can be explained by the fact that the two components of the external force influence the deformable model in different regions of the space.

5. Conclusion

We proposed an approach to integrate a new type of constraints, based on spatial relations, in deformable models. Spatial relations are represented using fuzzy subsets of the 3D space. The integration is based on the construction of new external forces derived from a fuzzy set. Three different construction methods were proposed. The forces possess the properties needed to make the deformable model converge towards the regions where the relations are satisfied. In the present work, we used distance and directional relations but the proposed framework is general and can handle any type of relation represented by a spatial fuzzy set. In particular, it is not restricted to basic relations but can be used with complex relationships such as “between” for which fuzzy spatial representations were proposed [14]. Moreover, the framework is valid in two or three dimensions and does not depend on the choices made concerning the design of the deformable model. We introduced a training step to estimate the parameters involved in the definition of the spatial relations, making the procedure robust to the choice of the trade-off between the two terms of the external force. However, it should be noted that the spatial relations are defined from prior anatomical knowledge and not directly extracted from the training set. The training step is thus not mandatory and the parameters can also be set manually, as was done for the thalamus in our experiments.

This framework has been applied to the segmentation of brain subcortical structures in MRI including the ventricles, the caudate nuclei and the thalami. The quantitative validation performed for the caudate nucleus showed that the method reaches a high degree of accuracy. Our experiments demonstrated that the introduction of spatial relations in a deformable model can substantially improve the segmentation of objects with ill-defined boundaries. The results were not sensitive to the tuning of the parameters, the most important ones being estimated using a training phase. However, the objective of this paper was primarily to propose an original methodology for integrating spatial relations into deformable models and to demonstrate its validity and utility through a brain segmentation application. For the particular

application of brain structure segmentation, the robustness of the approach should be quantitatively assessed in a larger population and with different acquisition protocols.

The main perspectives of this work are the combination of spatial relations with shape constraints in a deformable model and the simultaneous segmentation of different objects. To this purpose, it would be useful to propose methods allowing to update the fuzzy sets corresponding to spatial relations during the evolution process, avoiding a complete recomputation at each step. Finally, the proposed framework is general and can be applied to other structures or images. Potential applications concern medical imaging (we have applied some principles of the methodology to the segmentation of thoracic and abdominal structures in CT and PET images [51]) or the tracking of facial features.

Acknowledgments

We would like to thank Dr. Hasboun (CHU La Pitié-Salpêtrière) for providing the images and the descriptions of brain structures.

References

[1] L. Vieu, Spatial representation and reasoning in artificial intelligence, in: O. Stock (Ed.), Spatial and Temporal Reasoning, Kluwer, Dordrecht, 1997, pp. 5–41.
[2] Y. Mathet, New paradigms in space and motion, in: Proceedings of the European Conference on Artificial Intelligence ECAI 2000, Workshop on Spatio-temporal Reasoning, Berlin, 2000, pp. 30–37.
[3] D. Mark, M. Egenhofer, Modeling spatial relations between lines and regions: combining formal mathematical models and human subject testing, Cartography Geographic Inf. Syst. 21 (4) (1994) 195–212.
[4] B. Kuipers, The spatial semantic hierarchy, Artif. Intell. 119 (1–2) (2000) 191–233.
[5] J. Keller, X. Wang, A fuzzy rule-based approach to scene description involving spatial relationships, Comput. Vision Image Understanding 80 (2000) 21–41.
[6] M. Skubic, S. Blisard, C. Bailey, J. Adams, P. Matsakis, Qualitative analysis of sketched route maps: translating a sketch into linguistic descriptions, IEEE Trans. Syst. Man, Cybern.—Part B: Cybern. 34 (2) (2004) 1275–1282.
[7] F. Le Ber, L. Mangelick, A formal representation of landscape spatial patterns to analyze satellite images, AI Appl. 12 (1–3) (1998) 51–59.
[8] R. Cesar, E. Bengoetxea, I. Bloch, Inexact graph matching using stochastic optimization techniques for facial feature recognition, in: Proceedings of the International Conference on Pattern Recognition ICPR 2002, vol. 2, Québec, Canada, 2002, pp. 465–468.
[9] S. Waxman, Correlative Neuroanatomy, 24th ed., McGraw-Hill, New York, 2000.
[10] I. Bloch, H. Maître, M. Anvari, Fuzzy adjacency between image objects, Int. J. Uncertainty Fuzziness Knowledge-Based Syst. 5 (6) (1997) 615–653.
[11] I. Bloch, On fuzzy distances and their use in image processing under imprecision, Pattern Recognition 32 (11) (1999) 1873–1895.
[12] I. Bloch, Fuzzy relative position between objects in image processing: a morphological approach, IEEE Trans. Pattern Anal. Mach. Intell. 21 (7) (1999) 657–664.
[13] O. Colliot, A. Tuzikov, R. Cesar, I. Bloch, Approximate reflectional symmetries of fuzzy objects with an application in model-based object recognition, Fuzzy Sets Syst. 147 (1) (2004) 141–163.
[14] I. Bloch, O. Colliot, R.M. Cesar, On the ternary spatial relation "between", IEEE Trans. Syst. Man Cybern., Part B: Cybern. 36 (2) (2006) 312–327.
[15] X. Wang, J. Keller, P. Gader, Using spatial relationships as features in object recognition, in: Proceedings of the Annual Meeting of the North American Fuzzy Information Processing Society NAFIPS 1997, Syracuse, NY, USA, 1997, pp. 160–165.
[16] T. Géraud, Segmentation des structures internes du cerveau en imagerie par résonance magnétique tridimensionnelle, Ph.D. thesis, Telecom Paris, 1998.
[17] T. Géraud, I. Bloch, H. Maître, Atlas-guided recognition of cerebral structures in MRI using fusion of fuzzy structural information, in: CIMAF'99 Symposium on Artificial Intelligence, La Havana, Cuba, 1999, pp. 99–106.
[18] I. Bloch, T. Géraud, H. Maître, Representation and fusion of heterogeneous fuzzy information in the 3D space for model-based structural recognition—application to 3D brain imaging, Artif. Intell. 148 (2003) 141–175.
[19] V. Barra, J.-Y. Boire, Automatic segmentation of subcortical brain structures in MR images using information fusion, IEEE Trans. Med. Imaging 20 (7) (2001) 549–558.
[20] D. Collins, C. Holmes, T. Peters, A. Evans, Automatic 3D model-based neuroanatomical segmentation, Hum. Brain Mapp. 3 (3) (1995) 190–208.
[21] B. Dawant, S. Hartmann, J.-P. Thirion, F. Maes, D. Vandermeulen, P. Demaerel, Automatic segmentation of internal structures of the head using a combination of similarity and free-form transformations: part I, methodology and validation on normal subjects, IEEE Trans. Med. Imaging 18 (10) (1999) 909–916.
[22] T. Cootes, D. Cooper, C. Taylor, J. Graham, Active shape models—their training and application, Comput. Vision Image Understanding 61 (1) (1995) 38–59.
[23] M. Kass, A. Witkin, D. Terzopoulos, Snakes: active contour models, Int. J. Comput. Vision 1 (4) (1987) 321–331.
[24] C. Xu, D. Pham, J. Prince, Medical image segmentation using deformable models, in: J. Fitzpatrick, M. Sonka (Eds.), Handbook of Medical Imaging, vol. 2, SPIE Press, 2000, pp. 129–174.
[25] L. Cohen, I. Cohen, Finite element methods for active contour models and balloons for 2D and 3D images, IEEE Trans. Pattern Anal. Mach. Intell. 15 (11) (1993) 1131–1147.
[26] C. Xu, J. Prince, Snakes, shapes and gradient vector flow, IEEE Trans. Image Process. 7 (3) (1998) 359–369.
[27] N. Paragios, R. Deriche, Geodesic active regions and level set methods for supervised texture segmentation, Int. J. Comput. Vision 46 (3) (2002) 223–247.
[28] D. Shen, E. Herskovits, C. Davatzikos, An adaptative-focus statistical shape model for segmentation and shape modeling of 3D brain structures, IEEE Trans. Med. Imaging 20 (4) (2001) 257–270.
[29] J. Montagnat, H. Delingette, N. Ayache, A review of deformable surfaces: topology, geometry and deformation, Image Vision Comput. 19 (2001) 1023–1040.
[30] C. Xu, D. Pham, M. Rettmann, D. Yu, J. Prince, Reconstruction of the human cerebral cortex from magnetic resonance images, IEEE Trans. Med. Imaging 18 (6) (1999) 467–480.
[31] A. Pitiot, H. Delingette, P. Thompson, N. Ayache, Expert knowledge-guided segmentation system for brain MRI, NeuroImage 23 (S1) (2004) 85–96.
[32] A. Varzi, Parts, wholes and part-whole relations: the prospects of mereotopology, Data Knowl. Eng. 20 (1996) 259–286.
[33] A. Cohn, Qualitative spatial representations, in: Proceedings of the International Joint Conference on Artificial Intelligence IJCAI 99 Workshop on Adaptive Spatial Representations of Dynamic Environments, 1999, pp. 33–52.
[34] K. Miyajima, A. Ralescu, Spatial organization in 2D segmented images: representation and recognition of primitive spatial relations, Fuzzy Sets Syst. 65 (2–3) (1994) 225–236.

[35] P. Matsakis, L. Wendling, A new way to represent the relative position between areal objects, IEEE Trans. Pattern Anal. Mach. Intell. 21 (7) (1999) 634–643.
[36] I. Bloch, Mathematical morphology and spatial relationships: quantitative, semi-quantitative and symbolic settings, in: L. Sztandera, P. Matsakis (Eds.), Applying Soft Computing in Defining Spatial Relationships, Physica Verlag, Springer, 2002, pp. 63–98.
[37] I. Bloch, Information combination operators for data fusion: a comparative review with classification, IEEE Trans. Syst. Man Cybern.—Part A 26 (1) (1996) 52–67.
[38] D. Dubois, H. Prade, Fuzzy Sets and Systems: Theory and Applications, Academic Press, New York, 1980.
[39] H. Delingette, General object reconstruction based on simplex meshes, Int. J. Comput. Vision 32 (2) (1999) 111–146.
[40] C. Xu, Deformable models with application to human cerebral cortex reconstruction in magnetic resonance images, Ph.D. thesis, Johns Hopkins University, 2000.
[41] O. Colliot, O. Camara, R. Dewynter, I. Bloch, Description of brain internal structures by means of spatial relations for MR image segmentation, in: Proceedings of the International Society of Optical Engineering, SPIE 2004 Medical Imaging, vol. 5370, San Diego, USA, 2004, pp. 444–455.
[42] R. Deriche, Using Canny's criteria to derive a recursively implemented optimal edge detector, Int. J. Comput. Vision 1 (2) (1987) 167–187.
[43] G. Gerig, O. Kubler, R. Kikinis, F. Jolesz, Nonlinear anisotropic filtering of MRI data, IEEE Trans. Med. Imaging 11 (2) (1992) 221–232.
[44] F. Poupon, Parcellisation systématique du cerveau en volumes d'intérêt. le cas des structures profondes, Ph.D. thesis, INSA Lyon, Lyon, France, December 1999.
[45] B. Piquet, C.T. Silva, A. Kaufman, Tetra-cubes: an algorithm to generate 3D isosurfaces based upon tetrahedra, in: Proceedings of the Brazilian Symposium on Computer Graphics and Image Processing SIBGRAPI 96, vol. 21, 1996, pp. 205–210.
[46] D. Collins, P. Neelin, T. Peters, A. Evans, Automatic 3D intersubject registration of MR volumetric data in standardized Talairach space, J. Comput.-Assisted Tomography 18 (1994) 192–205.
[47] J.-F. Mangin, Entropy minimization for automatic correction of intensity non uniformity, in: Proceedings of the Mathematical Methods in Biomedical Image Analysis MMBIA 2000, Hilton Head Island, SC, USA, 2000, pp. 162–169.
[48] J.-F. Mangin, O. Coulon, V. Frouin, Robust brain segmentation using histogram scale-space analysis and mathematical morphology, in: Proceedings of the Medical Image Computing and Computer-Assisted Intervention MICCAI 1998, vol. 1496, Cambridge, MA, USA, 1998, pp. 1230–1241.
[49] A. Zijdenbos, B. Dawant, R. Margolin, A. Palmer, Morphometric analysis of white matter lesions in MR images: method and validation, IEEE Trans. Med. Imaging 13 (4) (1994) 716–724.
[50] J.-H. Xue, S. Ruan, B. Moretti, M. Revenu, D. Bloyet, Knowledge-based segmentation and labelling of brain structures from MRI images, Pattern Recognition Lett. 22 (2001) 395–405.
[51] O. Camara, O. Colliot, I. Bloch, Computational modeling of thoracic and abdominal anatomy using spatial relationships for image segmentation, Real-Time Imaging 10 (4) (2004) 263–273.